Nonlinear Gyrokinetic Particle Simulation of Dissipative Trapped Electron Mode

C. Zhao[1], Y. Xiao*

[1]Inst. Fusion Theory and Simulation, Zhejiang Univ., Hangzhou 310027, P.R.C.

* (Corresponding author) Email: yxiao@zju.edu.cn

7/5/2018

Abstract

Electron turbulence induced by trapped electron mode has been widely studied. The dissipative trapped electron mode (DTEM) is an important candidate for tokamak edge turbulence. Nonlinear gyrokinetic particle simulations based on edge parameters are carried out to investigate the collisional effects on the nonlinear transport of DTEM turbulence. It is found the collisions can induce a low level radially inward electron transport for the DTEM turbulence, which is closely related to the phase difference between the radial turbulent motion and perturbed density fluctuation induced by collisional dissipation. We observe an inverse spectral cascade of the turbulence during the nonlinear DTEM saturation, which is caused by quasimode scattering induced by trapped electrons and important for determining the magnitude of turbulent transport. The nonlinear decorrelation time is found to be inversely proportional to the collisional frequency by gyrokinetic simulation, which is consistent with the predication of quasilinear theory.

I Introduction

Drift wave turbulence is one important candidate for the anomalous transport observed in tokamaks [1]. In particular, the turbulence driven by trapped electron mode (TEM) instabilities, namely the collisionless trapped electron mode (CTEM) and the dissipative trapped electron mode (DTEM), can be responsible for the electron anomalous transport in the tokamak plasmas [2][3]. The CTEM, which is excited by the precessional resonance of the trapped electrons, has been studied both analytically and by gyrokinetic simulation [3][4][5][6][7][8][9][10]. On the other hand, the DTEM is relatively less investigated by the gyrokinetic simulation [10], especially for the nonlinear physics of the DTEM turbulence. Recently, the interest on

the DTEM has been revived by observation of the so-called edge coherent mode (ECM) in the EAST experiment as well as the code validation process by the C-Mod experiment [11][12].

It is a common practice that people interpret the nonlinear transport and turbulence in terms of the characteristics of the linear instability [11]. These kinds of practice sometimes are misleading due to the spectral cascade during the nonlinear saturation. For example, the CTEM turbulence is excited at short wavelength [6] but saturates at long wavelength due to spectral cascading [13]. The spectral cascading during the nonlinear saturation has been an important research area since decades ago for people to accurately predict the transport level in tokamaks [3].

In this work, we use the global gyrokinetic particle simulation code GTC (Gyrokinetic Toroidal Code) [14] to investigate the nonlinear physics for DTEM, particularly the radial particle transport and the spectral cascading. We discover radially inward particle transport driven by the DTEM turbulence, which favors the formation of the transport barrier and the pressure pedestal. We identify that the nonlinear decorrelation time is inversely proportional to collisional frequency, first by a quasilinear theory and then verified by the gyrokinetic simulation, which shows that the quasilinear theory is still a valid description for the nonlinear DTEM transport in the edge turbulence. The spectral cascading during nonlinear saturation is found to be an inverse cascade induced by trapped electron scattering, which shows a different trend from the traditional theory [3].

The rest of the paper is organized as follows. In Sec. II, we discuss the simulation model and parameters used. Then we show the nonlinear transport results for the DTEM in Sec. III. In Sec. IV we show the nonlinear spectral cascading results or the DTEM. Finally, conclusion and discussion are given in Sec. V.

II. Simulation model and parameters

The GTC code is a three-dimensional global gyrokinetic particle code for tokamak physics simulations, which uses the Boozer coordinates for realistic

magnetic field geometry [15]. This code invokes a nonlinear δf scheme [16] to simulate the drift wave turbulence, energetic particle physics and many other important physics topics associated with instability and transport in the tokamak [17][18]. The linear DTEM simulation has been successfully benchmarked in our recent work with the analytical theory that includes the pitch angle scattering collision [19].

In the GTC simulation, the particle distribution is composed of an equilibrium Maxwellian distribution F_0 and a perturbed distribution function δf. The perturbed part for the ion δf_i, and the non-adiabatic response δg_e, are solved through the nonlinear gyrokinetic equation [20] [21].

The δf method used in the GTC code efficiently limits the Monte Carlo noise associated with the discrete particles. We denote the particle weight w_i and w_e for the ion and electron respectively: $\mathrm{w}_i = \delta f_i / f_i$, $\mathrm{w}_e = \delta g_e / f_e$, which satisfies the following time evolution equation:

$$\frac{d}{dt} w_i = -(1-w_i)\left(\vec{v}_E \cdot \vec{\kappa} + \frac{q_i}{T_i} v_{\parallel} E_{\parallel} - \frac{q_i}{T_i} \vec{v}_d \cdot \nabla \delta\phi \right), \tag{1}$$

$$\begin{aligned} \frac{d}{dt} w_e = & -\left(1 - \frac{\delta f_e^{(0)}}{f_{0e}} - w_e \right) \\ & \times \left[\vec{v}_E \cdot \nabla \ln f_{0e}\big|_{v_\perp} - \frac{e}{T_e} \vec{v}_d \cdot \nabla \delta\phi + \frac{\partial}{\partial t} \frac{\delta f_e^{(0)}}{f_{0e}} + (\vec{v}_E + \vec{v}_d) \cdot \nabla \frac{\delta f_e^{(0)}}{f_{0e}} \right], \end{aligned} \tag{2}$$

where $\vec{v}_E = \vec{E} \times \vec{B} / B^2$ is the $\vec{E} \times \vec{B}$ drift velocity, $\vec{v}_d = m\left(v_\perp^2/2 + v_\parallel^2\right) \vec{B} \times \nabla B / eB^3$ is the magnetic drift velocity, $\kappa = \nabla \ln n_0 + (mv^2/2T - 3/2) \nabla \ln T_0$ and $d/dt = \partial/\partial t + \dot{\vec{x}}_g \cdot \nabla + \dot{v}_\parallel \partial/\partial v_\parallel$ is the gyro-averaged Vlasov operator, where $\dot{\vec{x}}_g = v_\parallel \vec{B}/B_0 + \vec{v}_E + \vec{v}_d$, $\dot{v}_\parallel = -\vec{B}^* / mB_0 \cdot (\mu \nabla B_0 + q \nabla \phi)$, and $\vec{B}^* = \vec{B} + B_0 v_\parallel / \Omega \nabla \times \vec{b}$.

The collisions on the electrons are dominated by the electron-ion collisions, which can be represented for simplicity by a pitch angle scattering operator, given by the following Monte-Carlo process [22][23]:

$$\xi_{n+1} = \xi_n \left(1-\nu_{ei}\Delta t\right) + \left(R_n - 0.5\right)\left[12\left(1-\xi_n^2\right)\nu_{ei}\Delta t\right]^{\frac{1}{2}}, \tag{3}$$

where $\xi = v_{\|}/v$ is the pitch angle of the particle, Δt is the time step, and R_n is a random number between 0 and 1.

In this work, we assume the concircular flux surface for simplicity. The basic simulation parameters are set as for a typical tokamak: $R_0 = 190\text{cm}$, $\varepsilon = a/R_0 = 0.3$, $B_0 = 1.70T$, $T_0 = 2200\text{ev}$, $T_i = T_e = T_0$, $n_0 = 4.0\times10^{13}\text{cm}^{-3}$, where R_0 is the main radius, B_0 is the on-axis equilibrium magnetic field, n_0, T_0 is the density and the temperature at the magnetic axis. The Fig. 1 shows the plasma profiles used in the nonlinear DTEM simulations, where a is the minor radius, r is the radial coordinate. In the simulation, we set steep gradients for plasma density and temperature profiles in the edge region ($0.8 \le r/a \le 1.0$), e.g.., $R_0/\partial_r \ln n_0 = 120$, $R_0/\partial_r \ln \mathrm{T}_e = 120$, $R_0/\partial_r \ln \mathrm{T}_i = 110$, to mimic the H-mode pressure profile of a typical tokamak. At the center of the pedestal, the plasma parameters are: $n_c = 1\times10^{13}$, $T_{ic} = 0.5kev$, $T_{ec} = 0.4kev$, $\nu_{ei} = 4.0C_s/R_0$, $\omega_{be} = v_{Te}/qR_0 = 20.0C_s/R_0$. The toroidal mesh for the electromagnetic field consists of 32 parallel grids on each flux surface and a set of unstructured poloidal mesh is set up with grid size about ρ_i in the radial and poloidal directions to simulate the short perpendicular wavelength modes. The normalized collisional frequency in this profile is $\nu_e^* \sim 1$ in tokamak edge, where the effective electron collisional frequency $\nu_e^* = \nu_{ei} qR_0 \left/ \left(v_{Te}\varepsilon^{3/2}\right)\right.$, v_{Te} is the electron thermal velocity and ν_{ei} is the typical electron-ion collisional frequency with $\nu_{ei} = n_i Z_i^2 e^4 \left/ \left(4\pi\varepsilon_0^2 m_e^2 v_{Te}^3\right)\right.$.

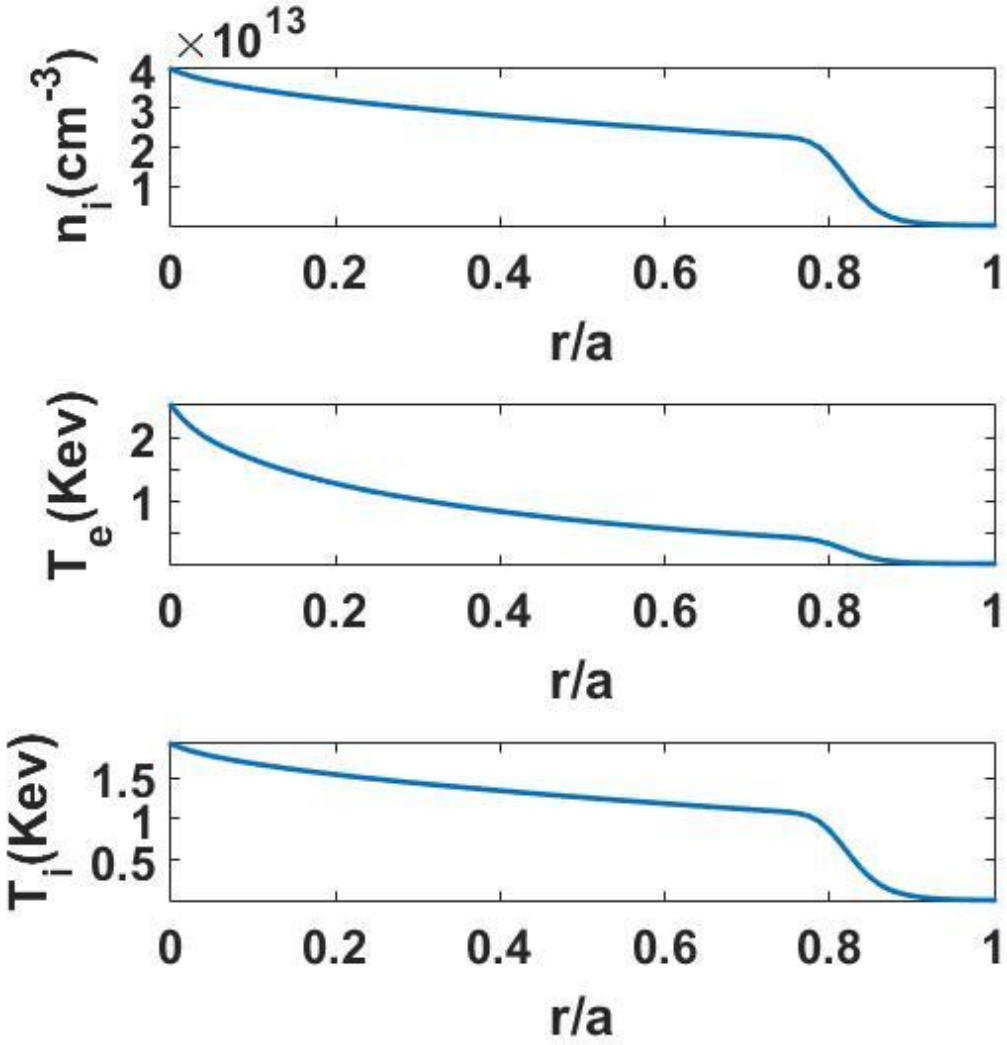

Figure 1: The plasma profiles used in the simulation for (a) ion density, (b) electron temperature, (c) ion temperature.

III. Nonlinear transports for DTEM simulations

The DTEM instability is caused by dissipative nonadiabatic response due to collisional trapping and detrapping of electrons. The linear growth rate of DTEM increases with the collisional frequency [24][19], which is different from the CTEM where the instability is driven by toroidal precessional resonance and the collisions play a damping role. Therefore, it is likely that the DTEM has a new saturation mechanism and transport behavior. Here we show nonlinear GTC simulation results

for the particle and energy transport to address these important physics issues for DTEM.

Fig. 2 shows the time history of the volume averaged electron particle and energy flux for DTEM, where the dashed line represents the simulation with the zonal flow, and the solid line represents the simulation without the zonal flow, and $t_s = tC_s/R_0$, $C_s = \sqrt{T_e/m_i}$ is the normalized time. We can see that there exists an radially inward particle flux in Fig. 2(a), while the heat flux is found radially outward in Fig. 2(b). As shown later in this section by a quasilinear theory, the inward direction of the electron flux is caused by the phase difference between perturbed potential and perturbed density due to the dissipation of collisions. It is known that zonal flow can reduce the turbulent transport for both ITG and CTEM turbulence [25]. It is thus interesting to observe the effect of zonal flow on the DTEM turbulence. From Fig 2 one can see that the zonal flow indeed affects the saturation process of the DTEM instability. However, the zonal flow does not have a significant effect on the saturated nonlinear DTEM transport level. This is because in the short or transient time scale, the zonal flow can be excited by the DTEM instability due to the smallness of the collisionless neoclassical polarization [25]; in the long and transport time scale, the zonal flow response is damped away due to the collisional neoclassical polarization [26].

Next, we try to investigate the transport mechanism for the DTEM turbulence and start with a quasilinear theory and compute the flux-surface averaged electron radial flux as:

$$\Gamma_{er} = \vec{\Gamma}_e \cdot \nabla r = \left\langle \delta n_e \delta v_{Er} \right\rangle = \int_0^{2\pi} \frac{d\theta}{2\pi} \left\langle \delta g_e \delta v_{Er} \right\rangle_v \quad , \tag{4}$$

where $\langle\ \rangle_v$ means integrate over the velocity space, $\delta v_{Er} = \frac{c}{B^2} \vec{B} \times \nabla \delta\phi \cdot \nabla r$ is the radial component of the $\mathbf{E}\times\mathbf{B}$ drift, δg_e is the non-adiabatic electron response in

the linear DTEM instability [19], which can be used to calculate the quasilinear turbulent transport:

$$\delta g_e = \frac{e\delta\phi}{T_e} Q(\mathrm{v}) \left(1 - \frac{J_0(a\sqrt{m})}{J_0(a)} \right) F_M , \tag{5}$$

where $Q(\mathrm{v}) = 1 - \omega_{*e}/\omega \left[1 + \eta_e \left(m_e v^2 / 2T_e - 3/2 \right) \right] \equiv 1 - \omega_{*e}^T / \omega$, J_0 is the zeroth order Bessel function, $a = 2(1+i)\sqrt{\omega\varepsilon/\nu_{ei}(\mathrm{v})}$, $m = E(1+\varepsilon) - \mu B_0 / 2\varepsilon E$ is the normalized electron velocity pitch angle, E is the electron kinetic energy, F_M is the Maxwellian distribution.

Choose the typical mode that maximize the mode amplitude in the nonlinear saturation phase, and combine Eq. (4) and Eq. (5), we can have:

$$\Gamma_{er} = \left\langle \frac{e\delta\phi}{T_e} Q(\mathrm{v}) \left(1 - \frac{J_0(a\sqrt{m})}{J_0(a)} \right) F_M \frac{c}{B^2} \vec{B} \times \nabla \delta\phi \cdot \nabla r \right\rangle . \tag{6}$$

Assuming $\nabla_\perp \delta\phi = \partial_\theta \delta\phi \nabla\theta + \partial_r \delta\phi \nabla r$, then Eq. (6) becomes:

$$\Gamma_{er} = \left\langle \frac{e\delta\phi}{T_e} \frac{J_0(a\sqrt{m})}{J_0(a)} F_M \frac{c}{B} i k_\theta \delta\phi \right\rangle - \left\langle \frac{e\delta\phi}{T_e} \frac{\omega_{*e}^T}{\omega} \frac{J_0(a\sqrt{m})}{J_0(a)} F_M \frac{c}{B} i k_\theta \delta\phi \right\rangle , \tag{7}$$

where the term $J_0(a\sqrt{m})/J_0(a)$ gives the perturbed density δn a phase shift from the perturbed electric potential $\delta\phi$ due to the collisional dissipation, which leads to the radially inward turbulent transport. If the $\nu_e^* \sim 1$, the numerical computation of Eq. (7) is shown as Fig. 3. we can find the flux can be nearly represented as $-4\times10^{-4}\nu_{ei}^{-1}$, when $0.5 < \nu_e^* < 2$, where the minus sign shows that the electron flux is radially inward. From this quasilinear point of view the particle flux is proportional to ν_{ei}^{-1} and the magnitude is restrained when the collision frequency is

large enough. We proceed to carry out gyrokinetic simulations using GTC for different collisionalities. In the simulation, we also find that the diffusivity is proportional to ν_{ei}^{-1} as shown in Fig. 4, which is consistent with the theoretical calculation in Fig. 3. This consistency suggests that the quasilinear theory is still a valid description for the nonlinear DTEM transport in the edge turbulence.

These preceding simulation and theory results show that the collisions can essentially change the transport feature of the TEM turbulence, i.e., the direction of the particle flux. It is known the radially inward flux is beneficial for the formation of transport barrier and the improvement the plasma confinement. Therefore, the DTEM turbulence can be a beneficial trigger for the L-H transition.

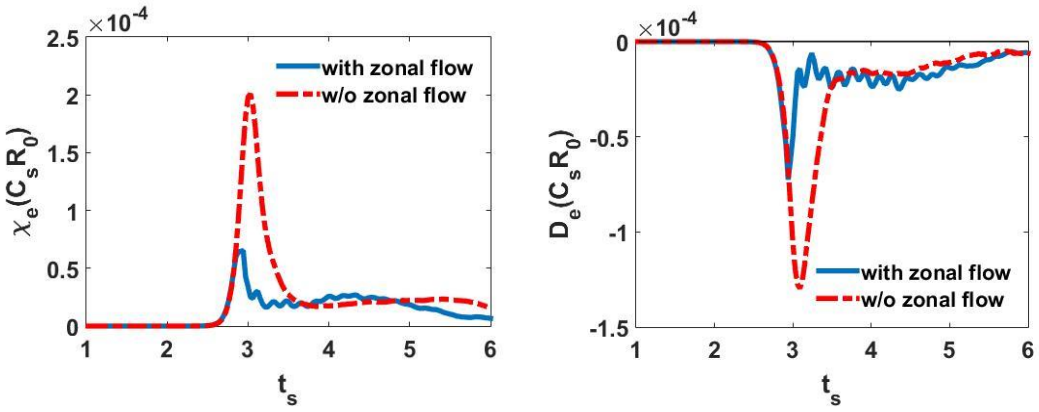

Figure 2: Time history of the volume averaged electron quantities: (a) particle diffusivity; (b) heat diffusivity.

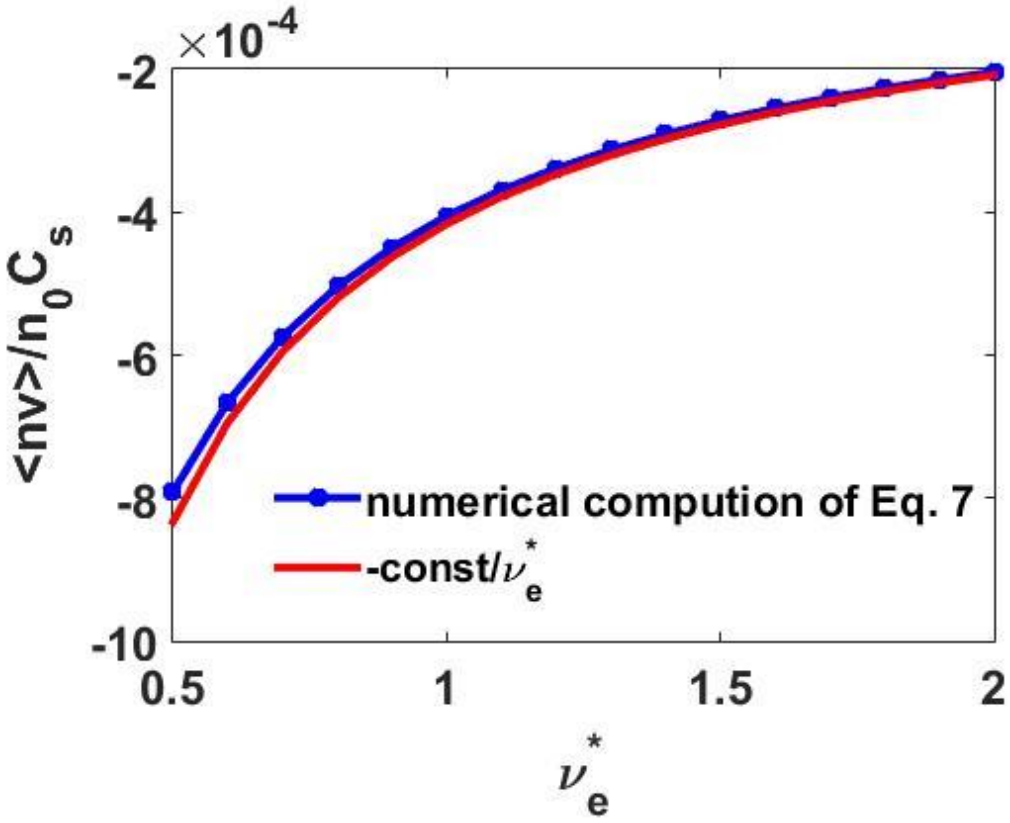

Figure 3: Electron particle flux $< \delta n_e \delta v_{Er} >$ vs. collisional frequency.

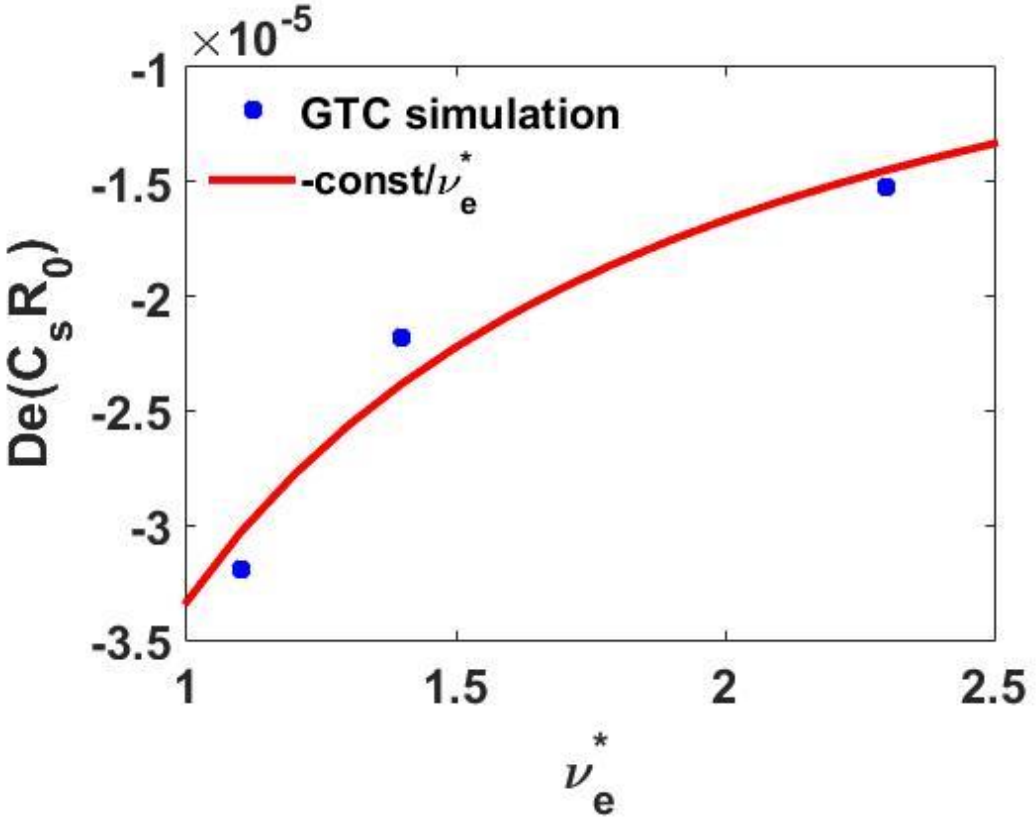

Figure 4: Electron diffusivity vs. collision frequency.

IV Nonlinear cascading for DTEM simulation

In Sec. III we have found an inward radial flux for the electrons in the DTEM and collisional TEM turbulence. Due to collisional damping, the zonal flow is not the dominant mechanism for the nonlinear saturation of DTEM turbulence. It is known the turbulent transport is closely related to the turbulence spectral since the spectral cascade can change the turbulence structure and affect the nonlinear saturation level and then turbulent transport [3]. It is thus desirable to investigate the nonlinear spectral cascade in the DTEM turbulence, as is shown in this section.

In order to observe the spectral cascading dynamics, the turbulence fluctuation can be decomposed into its Fourier components. The electric potential thus can be written as:

$$\phi\left(r,\theta,\zeta_0,t\right)=\sum_m\int dk_r\hat{\phi}_{k_r,m}\left(\zeta_0,t\right)e^{i\left(k_r r+m\theta\right)}, \qquad (8)$$

where $\hat{\phi}_{k_r,m}$ is the Fourier component of the electric potential at the toroidal angle ζ_0, k_r represents the radial wave vector, m is the poloidal mode number, θ is the poloidal angle . When the potential is translated into the Fourier space, we can plot $\left|\hat{\phi}_{k_r,m}\right|^2$ to find potential energy distribution. The time evolution of this distribution gives the spectral cascade of the turbulence.

Fig. 5 shows the two-dimensional contour for the potential energy for the DTEM turbulence in the edge region during the nonlinear saturation, where $k_\theta=m/r$ is the poloidal wave vector. All the four panels of Fig. 5 illustrate the potential energy distribution at different time steps during the nonlinear saturation in the radial and poloidal wave vector space. One can observe a clear spectral cascading in the poloidal direction while there is a slow normal cascade in the radial direction. We also note that k_r is the same size as k_θ, which satisfies the usual gyrokinetic assumption. Fig. 5(a) shows that, at the end of linear phase, the potential energy concentrates on

$k_\theta \rho_s \sim 0.4$, which is the most unstable mode in the linear phase. Fig. 5(b) shows that at the beginning of the nonlinear phase, the potential energy begins to transfer to a new wave ($k_\theta \rho_s \sim 0.05$). Then, the potential energy goes from short poloidal wavelength (higher $k_\theta \rho_s$) modes to the long poloidal wavelength (lower $k_\theta \rho_s$) modes, which are illustrated in Fig. 5(c) and Fig. 5(d). This process shows an inverse spectral cascading picture for the DTEM turbulence. Fig. 6 shows time history of the averaged poloidal mode number $\bar{m} = \sum_m m\hat{\phi}_m^2 \Big/ \sum_m \hat{\phi}_m^2$, where $\hat{\phi}_m$ is the poloidal Fourier component with mode number m at the flux surface r=a/2. As shown by the dotted solid line in Fig. 6, $\bar{m}$ becomes smaller during the nonlinear saturation, which suggests that the potential energy flows from the high mode number waves to the low mode number waves, and an inverse spectral cascading occurs during the DTEM nonlinear saturation (after $t_s = 2.5$). The averaged poloidal mode number $\bar{m} \sim 205$ ($k_\theta \rho_s \sim 0.4$) in the linear phase ($t_s < 2.5$) and decrease to $\bar{m} \sim 155$ ($k_\theta \rho_s \sim 0.3$) in the nonlinear saturation phase, which is consistent with Fig. 5.

Moreover, if we linearize the electron response while maintaining the nonlinear ion response to carry out another simulation with the same parameters, there does not exist any spectral cascading, as shown by the dot-dashed line in Fig. 6. But if we linearize the ion response in the simulation and keep the nonlinear electron response, the inverse spectral cascading remains unchanged, which is not shown in Fig. 6 for simplicity. These results suggest that the inverse spectral cascading in the DTEM is caused by the nonlinear wave interaction induced by the trapped electrons and has no relationship with the nonlinear ion Landau damping. We further note that the DTEM has a spectral cascading characteristics similar to that of CTEM [13], although the turbulence is driven by the collisions instead of the precessional resonance in the CTEM turbulence. It is this nonlinear scattering of quasimodes to longer wavelength modes induced by the trapped electrons, that leads to inverse spectral cascade and the saturation of the DTEM turbulence. However, the underlying nonlinear physics of

the spectral cascading in DTEM and how the collisions play a role requires further investigation.

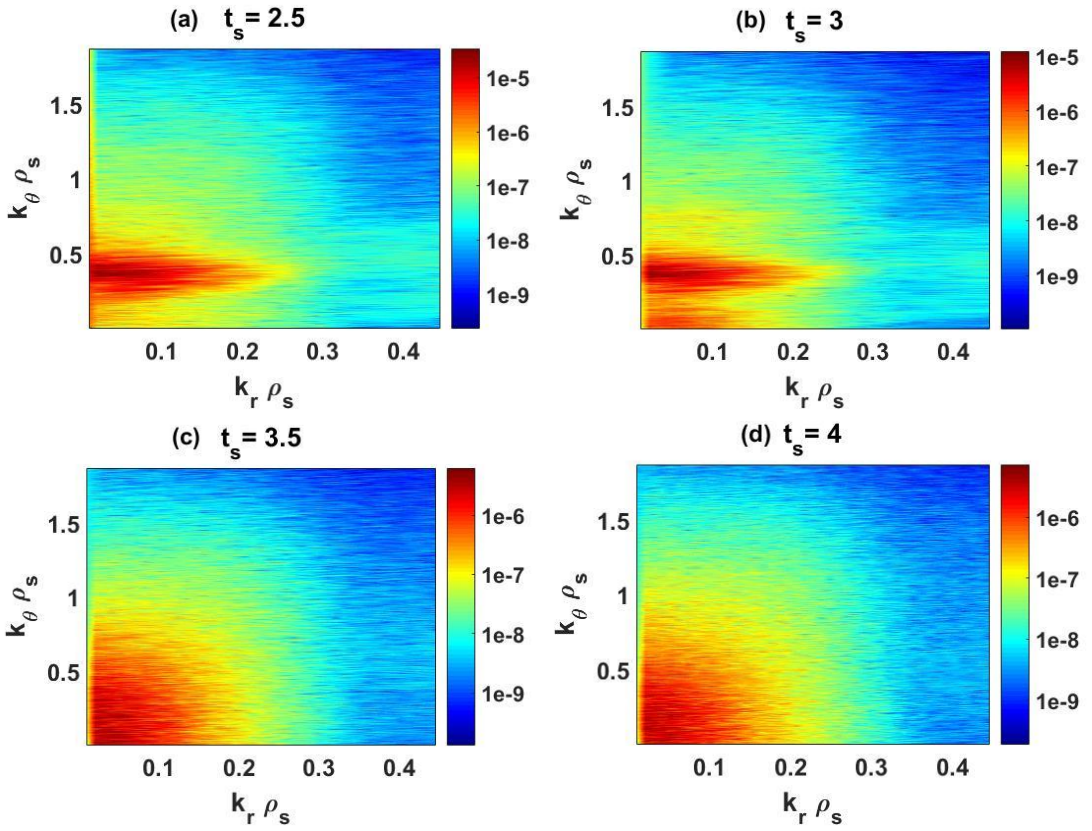

Figure 5: Evolution of 2D potential spectral $\left|\hat{\phi}_{k_r,m}\right|$ for the typical DTEM turbulence in the tokamak edge at (a) $t_s = 2.5$, (b) $t_s = 3.0$, (c) $t_s = 3.5$, (d) $t_s = 4.0$.

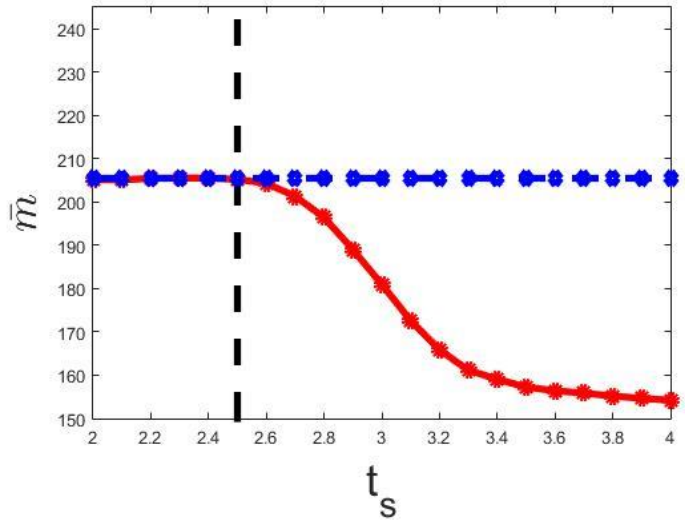

Figure 6: Averaged poloidal mode number $\bar{m}$ vs. time for the typical DTEM turbulence in the tokamak edge

V Conclusion and discussion

In this paper, we use the nonlinear gyrokinetic simulation by the GTC code to study the DTEM turbulence and the associated transport properties. It is found that in the DTEM turbulence the electron transport depends sensitively on the collisions. A radially inward particle flux is found by the self-consistent nonlinear simulation, which stems from the phase shift between the perturbed density and the electrostatic potential due to collisional dissipation and favors the formation of a transport barrier. We identify that the nonlinear decorrelation time is inversely proportional to collisional frequency, first by a quasilinear theory and then confirmed by the gyrokinetic simulation, which suggests that the quasilinear theory is a valid description for the nonlinear DTEM transport in the edge turbulence. It is further found that the inverse spectral cascading instead of the zonal flow leads to the saturation of the unstable modes and low level of turbulent transport in the DTEM turbulence. Although the driving mechanism for the DTEM turbulence is much different from that for CTEM, the DTEM turbulence has an inverse spectral cascading in the nonlinear saturation, which is similar to that in the CTEM turbulence. This

inverse spectral cascading in the DTEM turbulence is rooted from nonlinear quasimode scattering induced by the trapped electrons instead of the nonlinear ion Landau damping, which needs to be further investigated.

Acknowledgments

The authors thank Professor Liu Chen, Zhihong Lin and Guoyong Fu for useful discussions. The work is supported by National Magnetic Confinement Fusion Energy Research Program under Grant No. 2015GB110000, China NSFC under Grant No. 11575158, the Recruitment Program of Global Youth Experts.

Reference:

[1] W. Horton, Rev. Mod. Phys 71, 735 (1999).

[2] J. Adam, W. Tang, and P. Rutherford, Phys. Fluids 19, 561 (1976).

[3] L. Chen, R. Berger, J. Lominadze, M. Rosenbluth and P. Rutherford, Phys. Rev. Lett 39, 754 (1977).

[4] J. Lang, S. Parker, and Y. Chen, Phys. Plasmas 15, 055907 (2008).

[5] P. J. Catto and K. T. Tsang, Phys. Fluids 21, 1381 (1978).

[6] G. Rewoldt, Z. Lin, and Y. Idomura, Comput. Phys. Commun. 177, 775 (2007).

[7] Y. Xiao and Z. Lin, Phys. Plasmas 18, 110703 (2011).

[8] W. M. Tang, nucl. Fusion 18(8), 1089-1160 (1978).

[9] B. Coppi, and G. Rewoldt, Phys. Rev. Lett 32(22), 1329-1332 (1974).

[10] D. R. Ernst, R. S. Granetz, and M. H. Redi, Phys. Plasmas 11, 2637 (2004).

[11] H. Q. Wang and G.S.Xu, et al., Phys. Rev. Lett 112, 185004 (2014).

[12] D. R. Ernst, et al., Phys. Plasmas 23, 5 (2016).

[13] Y. Xiao, W. Zhang, S. Klasky and Z. Lin, Phys. Plasmas 17, 022302 (2010).

[14] Z. Lin, T. S. Hahm, S. Ethier, and W. M. Tang, Phys. Rev. Lett. 88, 195004 (2002).

[15] Y. Xiao, I. Holod, Z. X. Wang, Z. Lin, T. G. Zhang, Phys. Plasmas 22, 022516 (2015).

[16] A. M. Dimits, and W.W.Lee, J. Comput. Phys 107(2), 309-323 (1993).

[17] Y. Xiao, I. Holod, W. Zhang, S. Klasky and Z. Lin, Phys. Plasmas 17, 022302 (2010).

[18] W. Zhang, Z. Lin, and L. Chen, Phys. Rev. Lett 101, 095001 (2008).

[19] C. Zhao, T. Zhang, and Y.Xiao, Phys. Plasmas 24, 5 (2017).

[20] E. A. Frieman, and L. Chen, Phys. Fluids 25, 3 (1981).

[21] Z. Lin, Y. Nishimura, Y. Xiao, I. Holod, W. Zhang, and L. Chen, Plasma Phys. Controlled Fusion, 49, B163 (2007).

[22] Z. Lin, W. M. Tang, and W. W. Lee, Phys. Plasmas 2, 2975 (1995)..

[23] X. Q. Xu, and M. N. Rosenbluth, Phys. Fluids B 3, 627 (1991).

[24] K. T. Tsang, J. D. Callen, and P. J. catto, Phys. Fluids 20(12), 2113-2120 (1977)

[25] M. Rosenbluth and F. Hinton, Phys. Rev. Lett 80, 724 (1998).

[26] Z. Lin, T. S. Hahm, W. W. Lee, W. M. Tang, and P. H. Diamond, Phys. Rev. Lett. 83, 3645 (1999).